Mechanics of Turbulent Drag Reduction by Riblets

F. B. C. C. Sousa
A. P. Silva Freire
Programa de Engenharia Mecânica (COPPE/UFRJ), C.P. 68503, 21945-970, Rio de Janeiro, Brasil

J. B. R. Loureiro
Divisão Científica, Inmetro, Rio de Janeiro, Brasil

Abstract. *The present work studies the mechanics of turbulent drag reduction by streamwise aligned micro-grooved striations, also referred to as riblets. The effects of surface modification on flow separation over steep and smooth curved surfaces are investigated. Four types of two-dimensional surfaces are studied in the present work based on the morphometric parameters that describe the body of a blue whale. Local measurements of mean velocity and turbulence profiles are obtained through laser Doppler anemometry (LDA) and particle image velocimetry (PIV).*

Keywords: *Drag reduction, riblets, LDA, PIV.*

1. Introduction

The forces of resistance to the motion of a body are in most applications dominated by the viscous component. According to Frohnapfel et al. (2007) the viscous contribution to the total drag accounts to 50% on civil aviation, 90% on naval engineering and almost 100% on pipe flows.

In a near wall flow, most of the turbulent activity occurs at a very small scale, typically of the order of a few wall unit lengths, ν/u_*, where ν denotes the kinematic viscosity of the fluid and u_* the friction velocity. In fact, 80% of the total production of turbulence occurs near the wall, in the first 5% of the boundary layer (Lu and Willmarth, 1973). In this region, some structural organization can be observed, consisting of elongated, counter-rotating, streamwise vortices with diameters of approximately 40 wall units. These vortices appear to be sufficiently regular with an average spanwise wavelength of 80 to 100 wall units.

The existence of a well defined near wall structure dominated by low speed streaks suggests that passive and active methods could be used to control the properties of a boundary layer and, in special, to reduce viscous drag (Gad-el-Hak and Bandyopadhyay, 1994). To serve this purpose, several techniques have been studied in literature: polymer addition, compliant surfaces, wall transpiration, riblets and vortice generators (Gad-el-Hak, 2000).

The purpose of the present work is to study the mechanics of turbulent drag reduction by streamwise aligned micro-grooved striations, also referred to as riblets, for flow over curved surfaces. This is a problem that is rarely addressed in literature. Most works focus their attention on flow over flat surfaces (Karniadakis e Choi, 2003). Here, the effects of surface modification on flow separation over steep riblet surfaces are investigated. Four different surfaces are tested: (i) a symmetric smooth surface, (ii) an asymmetric smooth surface, (iii) a symmetric riblet surface and (iv) an asymmetric riblet surface.

The symmetric surfaces are very steep on the lee so that flow separation is promoted. The asymmetric surfaces, on the other hand, present a slow deceleration of the downflow so that separation is prevented. These two types of surface permit the assessment of drag reduction effects by the interplay between shape geometry and riblet walls.

Local measurements of mean velocity and turbulence profiles are obtained through laser Doppler anemometry (LDA) and particle image velocimetry (PIV).

2. Experiments

2.1 Geometry of surfaces

In Nature, the optimization of energy expenditure by aquatic mammals has benefited from evolutionary convergence. In addition to adaptations aimed at improving thrust, drag reduction plays an important role on energy savings (Fish and Lauder, 2006). Drag minimization is achieved by streamlining the shape of the body and appendages. However, the morphology of body, fluke and flipper vary greatly among species (Fish, 1993). The morphological characteristics of the blue whale *Balaenoptera musculus* suggests that drag reduction may be obtained by riblets.

The two types of two-dimensional surfaces studied in the present work are based on the morphometric parameters that describe the body of a blue whale (Becky et al., 2006). A symmetric steep curved surface is constructed from a reflection of the aft body shape of a blue whale around its apex, the point of maximum body thickness. The asymmetric smooth curved surfaces follow the geometry shown in red in Figure 1. The latter configuration is highly streamlined, thus

preventing flow separation.

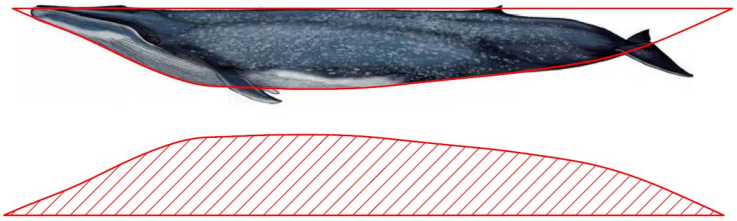

Figure 1. Morphometric features of a blue whale

Figure 2 shows the general forms of both surfaces: symmetric and asymmetric. The models were made in fiber-glass. The asymmetric model is 450 mm long, 500 mm wide and 50 mm thick.

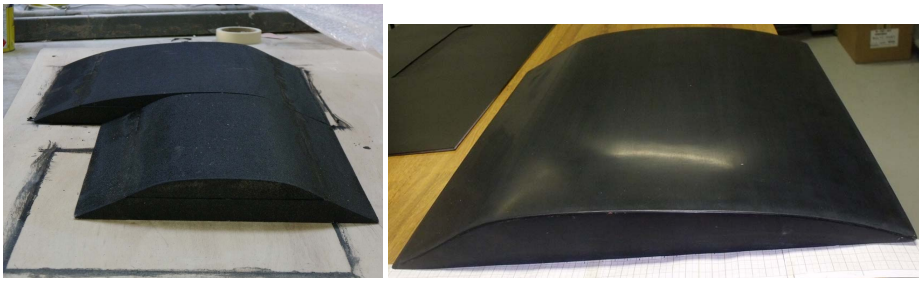

Figure 2. Model shapes: symmetric and asymmetric.

The cross-section of the riblets is given in Figure 3. A mechanical pencil is used to illustrate the size of the lengths involved.

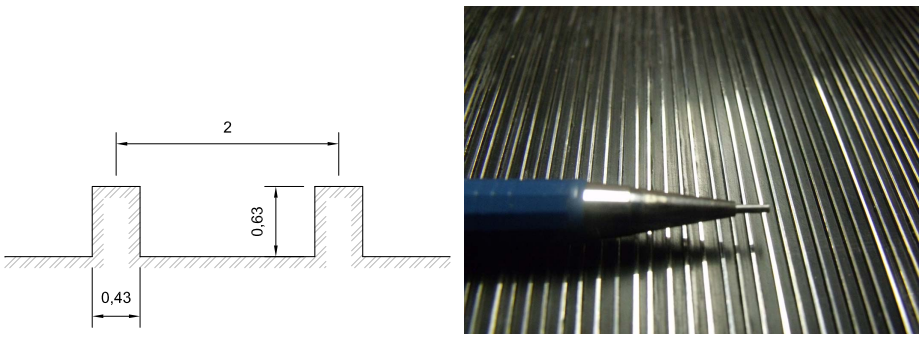

Figure 3. Geometry of riblets. Dimensions are in mm.

2.2 Wind tunnel and instrumentation

The experiments were carried out in the low-turbulence wind tunnel of the Laboratory of Flow Measurements of Inmetro. The tunnel is an open circuit tunnel with a test section of dimensions 500 mm x 500 mm x 8,000 mm. A general view of the wind tunnel is shown in Fig. 4.

Mean velocity and turbulence statistic data were obtained with a two component laser Doppler anemometer (LDA) and a two-dimensional particle image velocimeter (PIV).

The one-component Dantec laser-Doppler anemometry system used a 400 mW Ar-ion tube laser and was operated in the forwardcatter mode to measure mean and fluctuating velocity fields. A Bragg cell unit was used to introduce a digitally-controlled electronic shift in order to resolve the direction of the flow field and give correct measurements of near-zero mean velocities. The beams that emerged from the 60 mm diameter FiberFlow probe were made to pass through a beam translator and a beam expander with expansion ratio of 1.98. Table 1 below lists the main characteristics of the laser-Doppler system used. A series of LDA biases were avoided by adjusting the strictest parameters on the data processor and software.

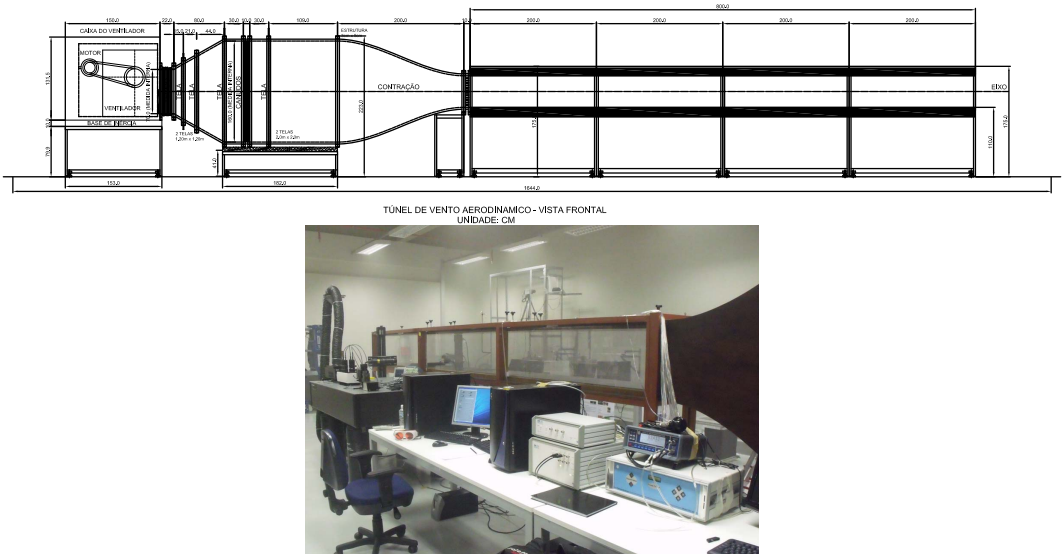

Figure 4. Wind tunnel: (a) schematic diagram, (b) general view.

Table 1. Main characteristics of the laser-Doppler system.

Wavelength	514.5 nm (green)
Half-angle between beams	2.8^o
Fringe spacing	5.28 μm
Beam spacing	71 mm
Beam diameter	2.65 mm
Focal distance	512.3 mm
Frequency of Bragg cell	40 MHz
Number of samples	100,000

In the experiments, the total number of samples for every point of velocity measurement was adjusted to ensure statistical independence between consecutive measurements as well as to furnish an interval of confidence of 95%. The overall uncertainty was calculated as described in ANSI/ASME (1986) and expressed in percentages of the free stream velocity, U_e (for the mean velocities) and the square of the friction velocity, (u_*^2) (for the Reynolds stress components). Typical uncertainties associated with the mean velocity data – U – are below $0.2\%U_e$. Regarding the second order moments, uncertainties were estimated to be $2.3\%u_*^2$.

The PIV measurements were performed with a two-dimensional Dantec system. The light source was furnished by a double pulsed Nd:YAG laser that produced short duration (10 ns) high energy (120 mJ) pulses of green light (532 nm). The collimated laser beam was transmitted through a cylindrical (15 mm) and a spherical (500 mm) lens to generate a 1 mm thick lightsheet. The reflected light was recorded at 5 Hz by a CCD camera with 1280 x 1024 pixels and 12-bit resolution. The cameras were fitted with a Nikkor 105 mm f/2.8D lenses. The air was seeded with a smoke generator. Image calibration was made by taking pictures of a reference target specially designed for the present purpose.

For all the measurements, computational conditions for the velocity vectors were fixed. Adaptive correlation (Dynamic Studio Software) has been processed on 32x32 pixels-size final interrogation windows, with 50% overlap, which gives 64x64 vectors. The pixel resolution is 6.45x6.45 μm. Particle image treatment using subpixel cell shifting and deformation, allowing bias and random error reduction. A widely accepted estimation of the absolute displacement error using these algorithms is 0.05 pixels. Different thresholds including signal-to-noise ratio and velocity vector magnitude were used as post-processing steps.

For both the LDA and PIV techniques, seeding was provided by a Laskin nozzle.

3. Results

The general flow pattern around the smooth symmetric surface is shown in Figure 5. The contour plots of mean velocity and turbulent shear stress were obtained through PIV. The flow is from left to right. The region of reverse flow is characterized by the blue dominated contour in the velocity plot and by the red/yellow dominated contour in the turbulent shear stress plot at the rear foot of the surface.

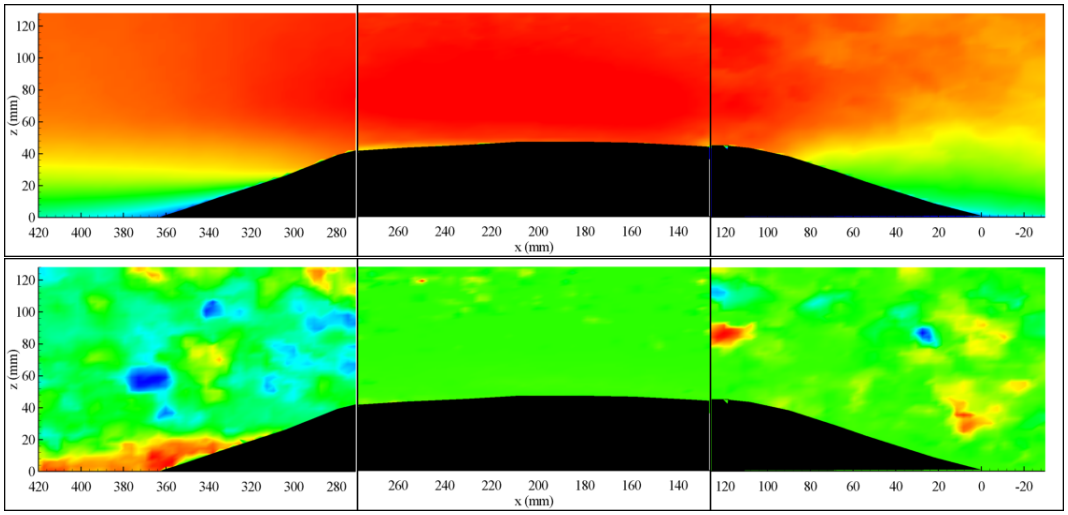

Figure 5. Contour plots: mean velocity (top) and turbulent shear stress (bottom).

The data of Figure 5 was particular important to determine the LDA-measurement positions. Four positions were selected (see inset in Figure 6a), two at the top of the surface, one at the separation point and one in the reverse region.

Measurements with LDA were only performed over the smooth surfaces. For the riblet surfaces, only pressure measurements were made.

The mean velocity profiles are shown in Figure 6. The striking feature is that Figure 6a does present a region of reverse flow (negative velocities) whereas Figure 6b presents only attached flow. The reference velocity U is the undisturbed external velocity upstream of the curved surfaces, 10 ms^{-1}. The velocity speed-up at the apex of the surfaces is observed at x = 175 and 205 mm. The strong external flow deceleration is apparent at positions x = 235 and 265 mm (Figure 6a).

The longitudinal turbulent shear stress is shown in Figure 7. The high shear rates in the mixing region between the separation bubble and the external flow increase σ_u $(= \overline{u'u'}/U_\delta^2)$ four times from its undisturbed values (Fig. 7a, x = 265 mm). The position of the peak in shear stress moves away from the wall.

Figure 7b shows that much lower turbulence levels are observed for the asymmetric curved surface, as compared to the symmetric surface. This is explained in simple terms by the slow flow deceleration that occurs over the asymmetric

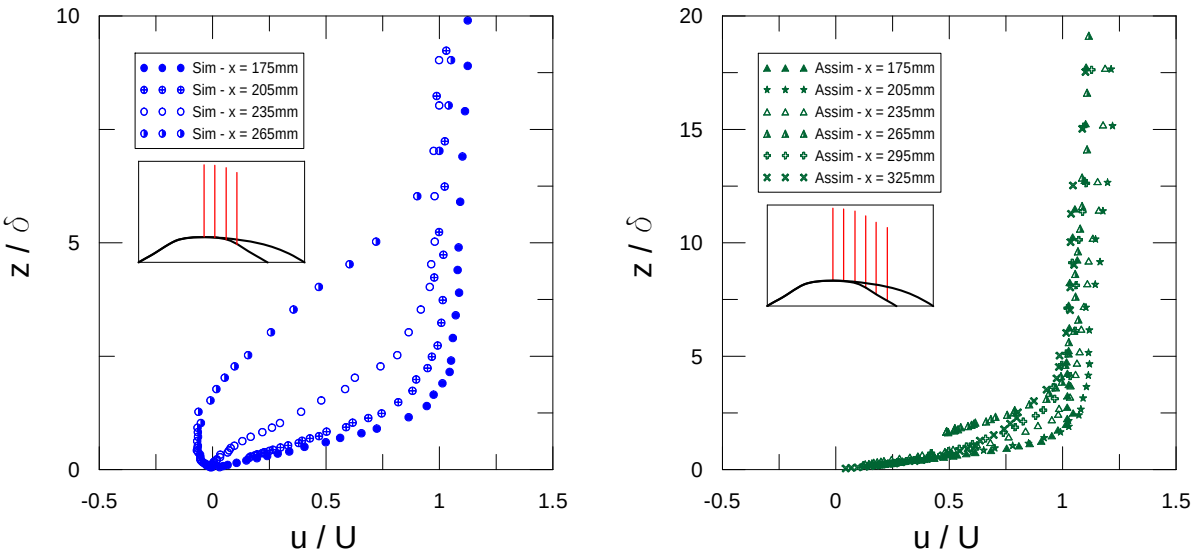

Figure 6. Mean velocity profiles: (a) symmetric surface (SIM), (b) asymmetric surface (ASSIM).

surface, which leads to less turbulence production due to the lower mean velocity gradients.

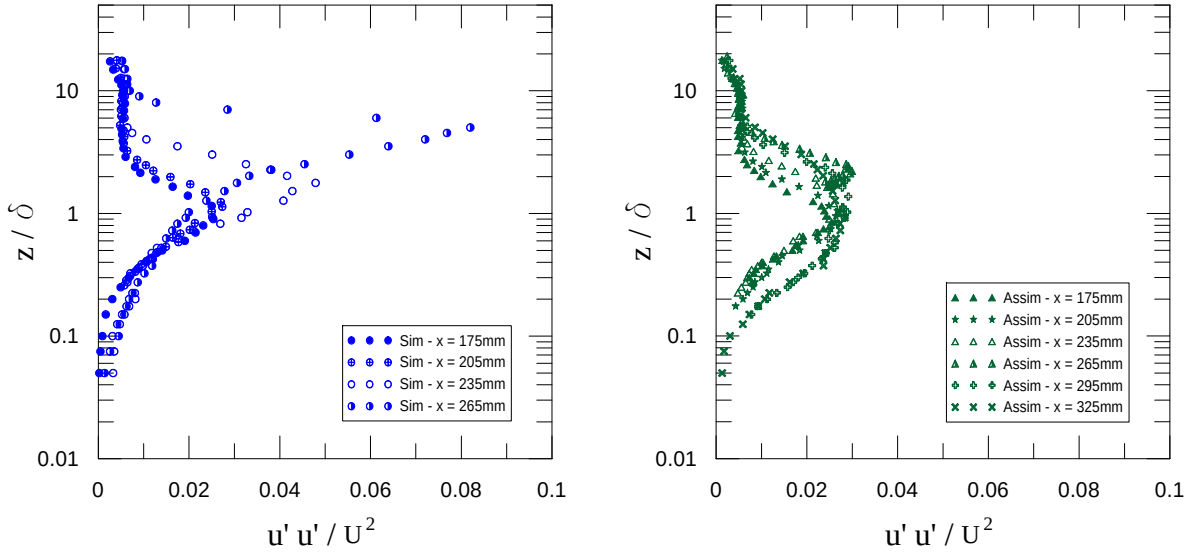

Figure 7. Longitudinal turbulent shear stress profiles: (a) symmetric surface (SIM), (b) asymmetric surface (ASSIM).

An important aspect for the successful use of riblets seems to be their ability to isolate the wall from the turbulence by maintaining laminar flow in the valleys. An assessment of the amount of turbulence that penetrates into the riblet cavities can be given by the third-order moments (S_u). Unfortunately, our LDA results only cover the smooth surface cases. These are reported next.

Flow regions where S_u is positive are associated with acceleration dominated velocity fluctuations resulting from the arrival of external high-speed fluid (sweep events) (Gad-el-Hak and Bandyopadhyay 1994).

The region of separated flow expands the region of violent positive fluctuations (Figure 8a). After the dip to negative values, no values of S_u close to those of a Gaussian distribution (S_u = 0) are recorded. At position x = 265 mm, negative values of S_u very close to the wall are observed. Over the asymmetric surface, the canonical behaviour of S_u for flow in boundary layers is observed (Figure 8b).

The flatness results shown in Figure 9 show a very high intermittent motion near the wall and in the outer layer. The region of reverse flow promotes highly intermittent motions that persist up to $z/\delta \approx 0.4$ (peak value of 10)(Figure 9a).

The overall drag performance of all four surfaces is presented in Figure 10 for Reynolds number (Re) up to 80,000. For Re lower than 15,000, the riblet surfaces present a decrease in C_d (= $\Delta P/(0.5\ \rho U^2)$, where ΔP is taken before and after the curved surfaces) of about 10%. In fact, in the range (10,000, 15,000) the riblet surfaces always perform better than

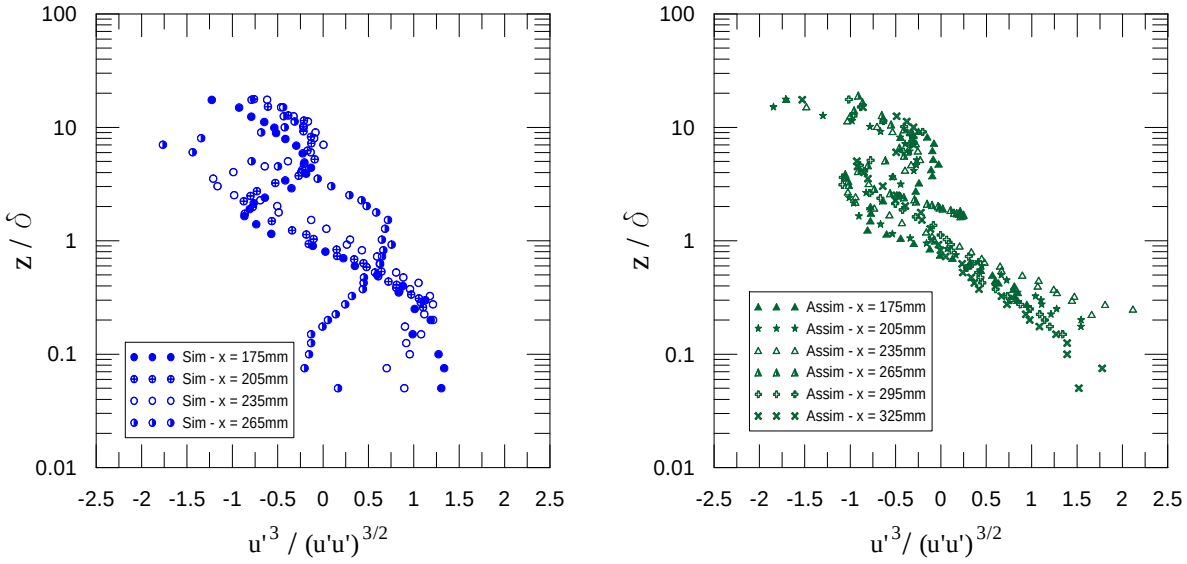

Figure 8. Skewness: (a) symmetric surface (SIM), (b) asymmetric surface (ASSIM).

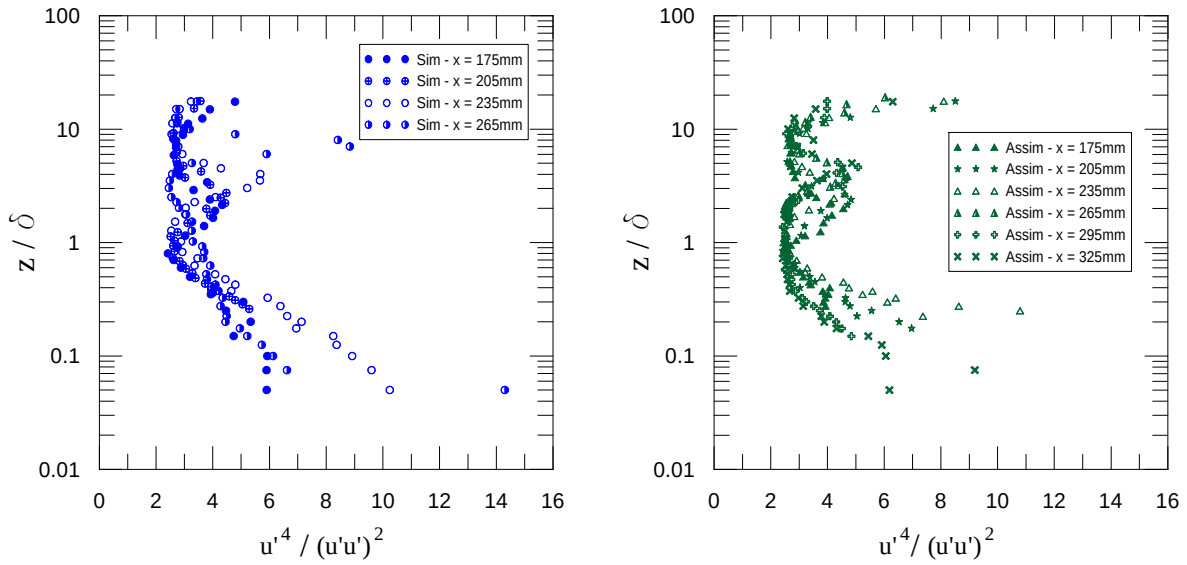

Figure 9. Flatness: (a) symmetric surface (SIM), (b) asymmetric surface (ASSIM).

the smooth surfaces. For the higher Re's, the riblet symmetric surface presents the worst aerodynamic performance. The worth point is the conclusion that the riblet asymmetric surface is the one that presents the best combined aerodynamic performance for high and low Re.

4. Final remarks

The present work has shown how riblet surfaces can be used to reduce drag in flows over curved surfaces with flow separation. The results show that for the whole Reynolds number domain, the asymmetric riblet surface performs better than all the other surfaces.

Further experiments are currently under way so that a complete PIV and LDA characterization of all four surfaces can be achieved. In addition, new types of surfaces will be tested.

Acknowledgements. FBCCS benefited from a Research Scholarship from the Brazilian Ministry of Education through Capes. APSF is grateful to the Brazilian National Research Council (CNPq) for the award of a Research Fellowship (Grant No 303982/2009-8). The work was financially supported by the Brazilian National Research Council (CNPq) through Grant No 473588/2009-9 and by the Rio de Janeiro Research Foundation (FAPERJ) through Grant E-26/170.005/2008.

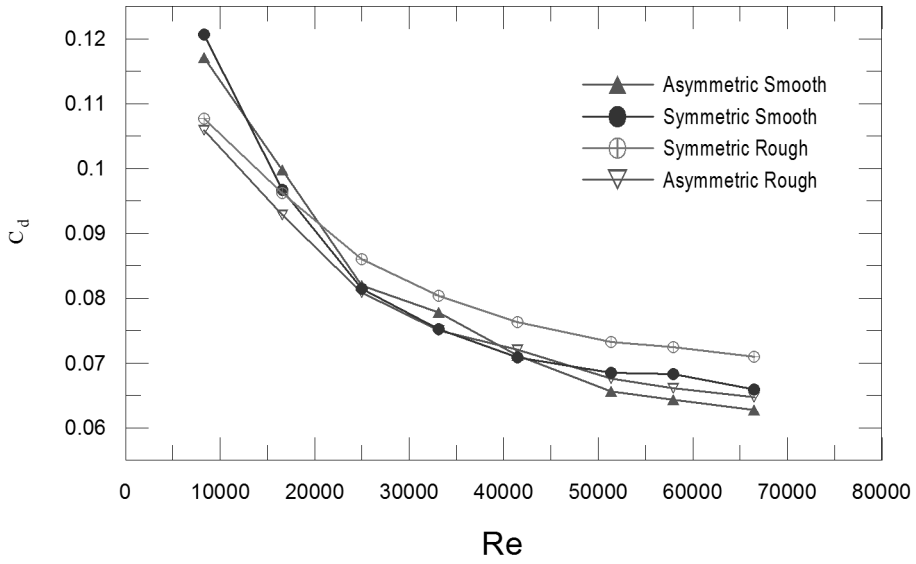

Figure 10. Drag coefficient.

JBRL is thankful to the Brazilian National Research Council (CNPq) for the financial support to this research through Grant 475759/2009-5.

5. REFERENCES

Becky, L.W., Winn, J. P. and Fish, F. E., 2006, "Morphological specialization of Baleen whales associated with hydrodynamic performance and ecological niche", J. Morphology, vol. 267, pp. 1284-1294.

Fish, F.E., 1993, "Influence of hydrodynamic design and propulsive mode on mammalian swimming energetics", Aust. J. ZOO., vol. 42, pp. 79-101.

Fish, F.E. and Lauder, G.V., 2006, "Passive and active flow control by swimming fishes and mammals", Annu. Rev. Fluid Mech., vol. 38, pp. 193Ű224.

Frohnapfel, B., Jovanovic, J. and Delgado, A., 2007, "Experimental investigations of turbulent drag reduction by surface-embedded grooves", J. Fluid Mechanics, vol. 590, pp. 107-116.

Gad-el-Hak, M. and Bandyopadhyay, P.R., 1994, "Reynolds number effects in wall-bounded turbulent flows", Appl Mech Rev, vol. 47, pp. 307Ű365.

Gad-el-Hak, M., 2000, "Flow Control: Passive, Active and Reactive Flow". Cambridge, CUP. Cambridge Univ. Press

Karniadakis, G.E. and Choi, K.-S., 2003, "Mechanisms on transverse motions in turbulent flows", Annu. Rev. Fluid Mech., vol. 35, pp. 45Ű62.

Lu, S.S. and Willmarth, W.W., 1973. "Measurements of the structure of the Reynolds stress in a turbulent boundary layer", J. Fluid Mech., vol. 60, pp. 481Ű511.